




Cite this: *RSC Adv.*, 2022, 12, 23183

Ce and P123 modified layered double hydroxide (LDH) composite for the synthesis of polypropylene glycol monomethyl ether†

Xiaoyan Cao, ^{ab} Lingxin Kong,^{ab} Zhenggui Gu ^{*ab} and Xiao Xu^{*a}

The application of recyclable heterogeneous catalysts in the production of polypropylene glycol monomethyl ether (MPPG) is of great significance to the green chemical industry. In this study, the CeO₂/MgAl-LDH(P123) composite was prepared using a nucleation/crystallization isolation method and aqueous reconstruction method, and CeO₂/MgAl-LDO(P123) solid base catalyst was prepared by calcination with it as precursor. Thereafter, the morphology, crystal structure, functional group, and thermal stability of the catalyst were characterized using scanning electron microscopy, X-ray diffraction, Fourier-transform infrared spectroscopy, Brunauer–Emmett–Teller analysis, temperature-programmed desorption of carbon dioxide, thermogravimetry, and X-ray photoelectron spectroscopy. The results showed that the catalyst had a larger specific surface area, pore size and pore volume and more basic sites, providing sufficient catalytic activity for the polymerization process. The experimental results for the fabrication of MPPG using CeO₂/MgAl-LDO(P123) as catalyst and methanol and propylene oxide as reaction raw materials showed that the conversion of propylene oxide reached 92.04% and the molecular weight of MPPG was 405 under the optimal reaction conditions. Moreover, the conversion of propylene oxide was maintained above 83.69% after the catalyst was reused six times. This study offers a new prospect for the green synthesis of MPPG products.

Received 16th June 2022
Accepted 1st August 2022

DOI: 10.1039/d2ra03716e

rsc.li/rsc-advances

1 Introduction

Polypropylene glycol monomethyl ether (MPPG) is widely used in the ink printing industry, surfactant industry and many other fields.¹ Usually, methanol is used as the initiator, and PO is used as the monomer. In polyether production based on the catalytic mechanism of anionic polymerization, the traditional homogeneous catalysts (such as NaOH, KOH and triethylamine aqueous solution) have high catalytic activity,² while the post-treatment process of the product will generate a large amount of waste liquid and salt, causing environmental pollution and equipment corrosion. Therefore, in order to satisfy the needs of green industrial production, the use of heterogeneous catalysts instead of traditional homogeneous catalysts has attracted more and more attention from researchers.

Layered double hydroxide (LDHs) belongs to a class of two-dimensional layered anionic clays, also known as hydrotalcite-like compounds, and its general chemical formula is

$[M^{II}_{(1-x)}M^{III}_x(OH)_2]^{x+}[A^{n-}]_{x/n} \cdot mH_2O$.^{3–6} Further, when $0.2 < x < 0.33$, the prepared LDHs material has high purity and complete crystal phase.⁷ The development of such materials became active in the 1940s after systematic studies of their physical properties.^{8,9} Since it has a two-dimensional layer structure and can exchange interlayer anions, it can be applied to many fields, such as acid–base catalysis, photocatalysis, point catalysis, catalyst carriers, wastewater treatment and pharmaceutical carriers, providing new ideas for research in the direction of heterogeneous catalysis.^{10–12}

The layered cations of LDHs are richly selective and an orderly and homogeneous distribution on the layer, and by calcination at a certain temperature, LDHs materials will undergo structural transformation to form composite layered double oxides (LDOs) with higher surface area and specific acid–base sites on the surface.^{13,14} Meanwhile, another effective way to control the specific surface area and dispersion is the template method. As a typical nonionic triblock copolymer, P123 has a clear role in guiding the mesoporous structure of LDHs materials due to its good “structure-directed behavior”. In the aqueous solution of P123, different micelle morphologies (e.g., cubic, hexagonal or lamellar morphologies) appear for different P123 concentrations.^{15,16} Wang *et al.*¹⁷ reported the preparation of mesoporous LDOs by a soft template method. Mg–Al layered double hydroxides with P123 as the template

^aSchool of Chemistry and Materials Science, Nanjing Normal University, Nanjing 210023, China. E-mail: 07160@njnu.edu.cn; 211102103@njnu.edu.cn

^bJiangsu Provincial Key Laboratory of Materials Cycling and Pollution Control, Nanjing Normal University, Nanjing 210023, China

† Electronic supplementary information (ESI) available. See <https://doi.org/10.1039/d2ra03716e>



were synthesized by using different amounts of P123. Due to their mesoporous nature, these unique composite metal oxides are promising for application as drug or catalyst carriers.

Cerium (Ce) is the most abundant element among rare earth metals, and its main oxide forms are Ce_2O_3 and CeO_2 , and CeO_2 is more stable at room temperature and pressure. Studies have shown that the surface of CeO_2 has both acidic and basic sites, and its basic number is more than that of MgO and ZrO_2 , mainly in the form of weak and medium bases.¹⁸ Currently, many scholars have introduced Ce into LDHs to prepare composites, which showed good performance in photocatalysis, base catalysis, and redox reactions.¹⁹ Jiang *et al.*²⁰ discussed the Mg–Al hydrotalcite (HT) catalysts with different cerium doping amount and used them for propionate ketonation. Under mild reaction conditions (350 °C), $\text{Mg}_3\text{Al}_{0.9}\text{Ce}_{0.1}$ exhibited the highest ketonization activity (90.6% propionic acid conversion). The strong interaction between CeO_2 and HT resulted the enhancement of redox properties and modification of acid–base sites, thereby facilitated the ketonization reaction. Nayak *et al.*²¹ designed the $\text{CeO}_2(x\%)/\text{MgAl-LDH}$ composite photocatalysts by dispersing CeO_2 on the surface of MgAl-LDH to improve the visible light capture ability of MgAl-LDH. The results showed that the band gap energy of the composites was tuned in the range from MgAl-LDH to $\text{CeO}_2(x\%)/\text{MgAl-LDH}$. Denis *et al.*²² modified the basicity of Zn–Al hydrotalcite-type materials by incorporating Ce into its structure and used it as a heterogeneous catalyst for soybean oil conversion. The results showed that with the addition of Ce, the basic site strength and special surface area of the ZnAl–Ce samples were increased, thereby improved their catalytic activity. However, the current studies on the base-catalytic performance of P123 template-modified and Ce-doped LDHs are very limited.

In this study, the P123 and Ce doped modified $\text{CeO}_2/\text{MgAl-LDH(P123)}$ was successfully prepared *via* a two-step nucleation/crystallization isolation method and aqueous reconstruction method, and calcined it as precursors to obtain $\text{CeO}_2/\text{MgAl-LDO(P123)}$ solid base catalyst. The mechanism diagram for $\text{CeO}_2/\text{MgAl-LDO(P123)}$ forming was shown in Fig. S1.† In addition, the amount of modifier P123 addition and the doping of Ce elements were discussed. Finally, the catalytic activity of $\text{CeO}_2/\text{MgAl-LDH(P123)}$ was evaluated in the synthesis of MPPG using methanol and PO for the first time. This research could provide a new strategy for green industrial applications of MPPG production with heterogeneous base catalysts.

2 Experimental section

2.1 Materials

All chemicals used in this work were of analytical grade and obtained from commercial sources. PO and methanol (CH_3OH) were purchased from Shanghai Lingfeng Chemical Reagent Co., Ltd, whereas Magnesium nitrate hexahydrate ($\text{Mg}(\text{NO}_3)_2 \cdot 6\text{H}_2\text{O}$), cerium nitrate hexahydrate ($\text{Ce}(\text{NO}_3)_3 \cdot 6\text{H}_2\text{O}$), aluminum nitrate hexahydrate ($\text{Al}(\text{NO}_3)_3 \cdot 9\text{H}_2\text{O}$), sodium hydroxide (NaOH) and ethanol ($\text{C}_2\text{H}_5\text{OH}$) were purchased from Sinopharm Chemical Reagent Co., Ltd. Poly(ethylene glycol)-

block-poly(propylene glycol)-*block*-poly(ethylene glycol) (P123) were purchased from Aladdin.

2.2 Preparation of MgAl-LDH and MgAl-LDH(P123)

P123(1.5 g) was dissolved in distilled water (100 ml) to form a P123 solution. $\text{Mg}(\text{NO}_3)_2 \cdot 6\text{H}_2\text{O}$ (0.075 mol) and $\text{Al}(\text{NO}_3)_3 \cdot 9\text{H}_2\text{O}$ (0.025 mol) were dissolved in P123 solution and stirred well. Then this mixed nitrate solution was slowly dropped into the Na_2CO_3 solution, and the pH was made to 10.0 with NaOH solution (2.0 mol L^{-1}). Afterward, it was transferred to a hydrothermal kettle and treated for 18 h at 110 °C. Lastly, the precipitate was washed with distilled water to pH 7.0, and secondly washed with ethanol, and the filter cake was dried overnight. The sample prepared by the nucleation/crystallization isolation method was named MgAl-LDH(P123), and the mass ratio of P123/water was 1.5 wt%. Similarly, MgAl-LDH was obtained without the addition of P123 solution. Besides, the MgAl-LDO(P123) and MgAl-LDO were obtained through the calcination of their LDHs precursors at 550 °C for 6 h, respectively.

2.3 Preparation of $\text{CeO}_2/\text{MgAl-LDH}$ and $\text{CeO}_2/\text{MgAl-LDH(P123)}$

$\text{Ce}(\text{NO}_3)_3 \cdot 6\text{H}_2\text{O}$ (0.005 mol) was dissolved in distilled water (100 ml) to obtain solution A. MgAl-LDO(P123) powder (5 g) was put into solution A for stirring and immersion, and the pH was controlled at 10.0 with NaOH solution (2.0 mol L^{-1}). The obtained precipitate was washed with distilled water and ethanol to pH 7.0, and the filter cake was dried overnight. The resulting sample was named $\text{CeO}_2/\text{MgAl-LDH(P123)}$ catalyst. Afterward, the $\text{CeO}_2/\text{MgAl-LDO(P123)}$ was obtained by calcining its precursor. The whole process was repeated, changing the amount of P123 with the mass ratio of P123/water was 1.0%, 2.0% and 2.5%, and the obtained samples were named as $\text{CeO}_2/\text{MgAl-LDO(1.0\%P123)}$, $\text{CeO}_2/\text{MgAl-LDO(2.0\%P123)}$ and $\text{CeO}_2/\text{MgAl-LDO(2.5\%P123)}$, respectively. Besides, the $\text{CeO}_2/\text{MgAl-LDH}$ and $\text{CeO}_2/\text{MgAl-LDO}$ materials without P123 were prepared by the same aqueous reconstruction method.

2.4 Characterizations

Scanning electron microscopy (SEM) images were got using a JSM-5610LV microscope (JEOL, Ltd, Japan). The crystallinity of the as-prepared materials was analysed *via* X-ray powder diffraction (XRD) (D8 Advance, Bruker, Germany). Fourier transform infrared (FTIR) spectroscopy was performed using a IRAffinity-1S instrument (Shimadzu Company, Japan). The specific surface area and porosity were measured using N_2 sorption (ASAP 2020, Micromeritics Corporation, USA). X-ray photoelectron spectroscopy (XPS) was conducted on an AXIS Supra instrument (Kratos, Japan). The thermogravimetric (TG) analysis was performed on a TGA 4000 analyser (PerkinElmer, Inc., USA). The amount and strength of basic sites were obtained *via* temperature-programmed desorption of carbon dioxide using a AutoChem II 2920 Instrument (Micromeritics Corporation, USA).



2.5 Catalytic tests

The polymerization reaction was carried out with methanol as initiator and PO as monomer. A measured amount of initiator (methanol) and catalyst were first added to the autoclave and the reactor was sealed. Nitrogen gas was introduced to replace the air in the kettle to remove the air from the kettle. Next, a measured amount of PO was added to the reactor and the reaction pressure was maintained with nitrogen. The reaction temperature and stirring speed were controlled and the polymerization reaction went through three stages: chain initiation, chain growth and chain transfer. When the pressure of the reaction system is basically constant, it indicates the end of the polymerization reaction. Then the temperature was cooled down by coolant, and it drops to 25 °C, the pressure in the kettle was evacuated and the reaction product was discharged. After the excess PO was removed from the product, the catalyst was removed *via* filtration to obtain the MPPG product. Finally, the products were analyzed using FTIR and ^1H NMR, national standard method and gel chromatography (GPC). The conversion of PO was calculated by eqn (1), where m_{PO_1} is the mass of PO in the feed, and m_{PO_2} is the mass of PO in the product.

$$X_{\text{PO}} = \frac{m_{\text{PO}_1} - m_{\text{PO}_2}}{m_{\text{PO}_1}} \quad (1)$$

3 Results and discussion

3.1 Structural and morphology characterizations

Fig. 1 and S2† show the SEM images of as-prepared materials. In Fig. 1a and c, the MgAl-LDH and MgAl-LDH (P123) materials both exhibited lamellar structures. Since the preparation method of rapid nucleation and crystallization isolation was adopted, the rate of nucleation and crystallization was effectively controlled, so the synthesized platelet structure was well defined and basically maintained the hexagonal structure of traditional hydrotalcite. Compared with MgAl-LDH, the lamellar particle size of MgAl-LDH(P123) is smaller, and the agglomeration state appears. This is because the introduction of P123 affects the distribution of MgAl-LDH(P123) nucleation and the growth range of lamellae.²⁰ The rehydration process reduces the order degree of LDH materials, and Ce element will enter the framework of the reconstructed hydrotalcite and increase the interlayer spacing. Therefore, the lamellar structure of $\text{CeO}_2/\text{MgAl-LDH(P123)}$ is not obvious, and the lamellae are loose and fragmented (Fig. 1e). Besides, in Fig. (1b, d and f), the layered structure of the LDOs samples obtained by calcination did not collapse obviously. The $\text{CeO}_2/\text{MgAl-LDO(P123)}$ sample has cluttered and irregular particles with more defects and corners at the edge of the structure, which may be beneficial for more active sites exposed.²³ The TEM images of MgAl-LDO(P123) and $\text{CeO}_2/\text{MgAl-LDO(P123)}$ are shown in Fig. S3.† The mesoporous structure in MgAl-LDO(P123) can be found from Fig. S3(a–c).† Furthermore, a large number of uniformly distributed black spots are present in $\text{CeO}_2/\text{MgAl-LDO(P123)}$ (Fig. S3(d and e)†). The crystal planes in Fig. S3(g)† were analyzed by Digital Micrograph, which correspond to the (111)

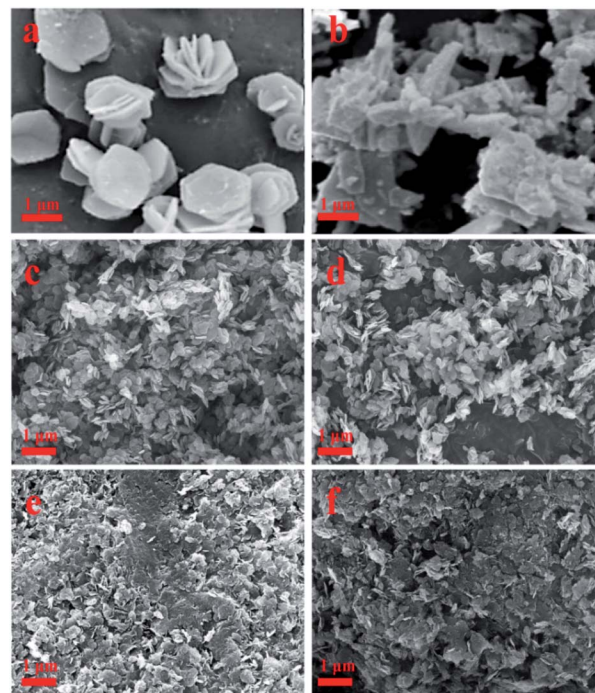


Fig. 1 SEM images of as-prepared materials: (a): MgAl-LDH; (b): MgAl-LDO; (c): MgAl-LDH (P123); (d): MgAl-LDO (P123); (e): $\text{CeO}_2/\text{MgAl-LDH}$ (P123); (f): $\text{CeO}_2/\text{MgAl-LDO}$ (P123).

and (311) planes of CeO_2 , respectively. On the other hand, the average particle size of CeO_2 grains distributed on the surface of LDO is about 4–5 nm as seen in Fig. S3(f).†

The XRD patterns of different as-prepared LDHs are displayed in Fig. 2. All the LDHs samples exhibited characteristic diffraction peaks of LDH (JCPDS PDF# 35-0965) at 11.0° , 23.0° , 34.0° , and 60.0° ,²⁴ showing that the introduction of Ce and P123 did not destroy the crystal structure of LDHs. The diffraction peaks at 28.7° , 33.2° , 47.7° , and 56.6° belong to the (111), (200), (220), and (311) crystal faces of the CeO_2 cubic fluorite structure, respectively (JCPDS PDF# 78-0694),²⁵ revealing that Ce elements were successfully introduced into the LDHs structure. Moreover, a crystallinity decrease can be observed with the introduction of Ce, which can be attributed to the inhibition of the enrichment of aluminum by Ce.

Fig. 3 shows the XRD patterns of LDOs. It can be found that the characteristic peaks of LDHs basically disappear completely, and $\text{CeO}_2/\text{MgAl-LDO}$ and $\text{CeO}_2/\text{MgAl-LDO(P123)}$ were mainly composed of amorphous Al_2O_3 , MgO and CeO_2 . The diffraction peaks at 37.5° , 43.0° and 62.0° were assigned to the (111), (200) and (220) crystal planes of MgO, respectively. Compared with MgAl-LDO, the intensity of the characteristic peak of $\text{CeO}_2/\text{MgAl-LDO(P123)}$ at 43.5° is weaker. Probably, it may due to the entry of CeO_2 into the lattice of LDOs, and on the other hand, the entry of MgO into the CeO_2 lattice could cause a formation of a new solid solution structure.²⁶ The absence of obvious diffraction peaks of heterogeneous species throughout the XRD spectra indicates that the as-prepared LDHs and LDOs have a certain degree of pure crystalline phase composition.



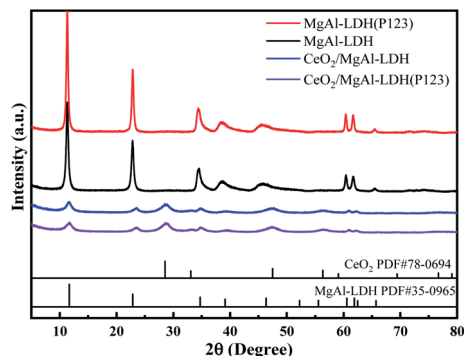


Fig. 2 XRD profiles of different LDHs materials.

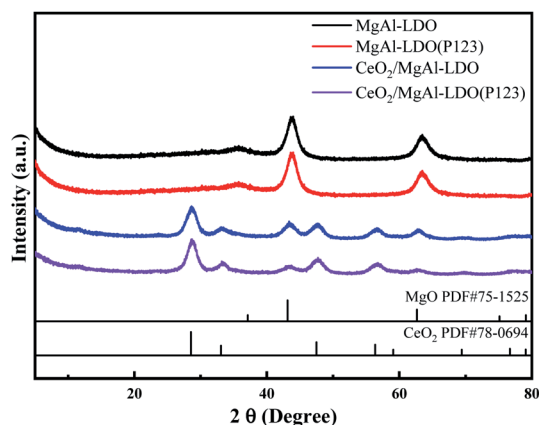


Fig. 3 XRD profiles of different LDOs materials.

Fig. 4 displays the FTIR spectra of LDHs and LDOs. The peaks at 3000–3500 cm^{-1} are corresponding to the stretching vibrational peaks of the O–H group, originating from the interlayer water molecules of the LDHs and the O–H connected to the metal cation bond in the hydroxide layer ($\text{Mg}/\text{Al}-\text{OH}$). The weak absorption peaks at 1620 cm^{-1} belong to the bending vibrations of interlayer water molecules, and these were typical of the infrared absorption peaks of LDHs. Due to the removal of

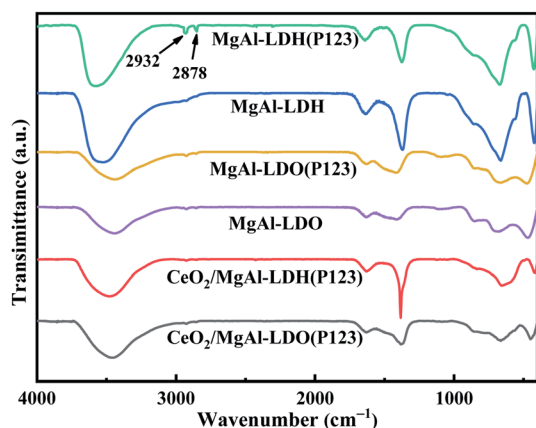


Fig. 4 FTIR spectra of as-prepared materials.

water in the calcination, there was a significant decrease in the peak height of both peaks. Compared with MgAl-LDH , the vibration peaks of MgAl-LDH(P123) at 2878 cm^{-1} and 2932 cm^{-1} are attributed to the alkyl stretching vibration peaks of P123,¹⁷ demonstrating the successful doping of P123 into LDHs. Furthermore, the characteristic peaks belonging to P123 disappeared after calcination revealed the successful removal of P123. The peaks between 500–750 cm^{-1} belong to the stretching vibration of the Ce–O bond and the asymmetric vibration of CO_3^{2-} appears at 1363 cm^{-1} .^{27,28} The peaks of the stretching vibrations of Mg–O and Al–O are present between 500–900 cm^{-1} , which belong to the lattice vibrations of the cationic layer.²⁹ Besides, from the IR spectra of different materials, it can be found that the structures of MgAl-LDH and $\text{CeO}_2/\text{MgAl-LDH(P123)}$ are almost the same, indicating that the introduction of P123 and Ce has almost no effect on the functional group structures of LDHs.

Usually, LDOs formed by calcination of LDHs materials have higher catalytic activity, and the calcination temperature can affect their morphology, structure and basicity.^{30,31} From Fig. 5, it can be seen that the TG curves of all the LDHs samples showed a significant three-step weight loss, with basically the same trend but different weight loss amplitudes.³² The removal of adsorbed water on the surface of LDHs and interlayer water corresponds to the weight loss before 200 °C. The second stage of weight loss was located between 200 °C and 400 °C, which was the loss of OH[−] group and partial CO_3^{2-} removal in the form of CO_2 . Among them, OH[−] was mainly removed in two forms in this range, one is the transformation of $\text{Al}^-(\text{OH})-\text{Mg}$ into $\text{Al}-\text{O}-\text{Mg}$, and the other was the transformation of $\text{Mg}^-(\text{OH})-\text{Mg}$ into $\text{Mg}-\text{O}-\text{Mg}$. The third stage of weight loss was between 410 °C and 550 °C, and the conversion of interlaminar CO_3^{2-} to CO_2 mainly occurs. After three weight loss stages, the overall material existed in an amorphous metastable mixed solid oxide form. The difference in the weight loss process of $\text{CeO}_2/\text{MgAl-LDO(P123)}$ is mainly due to the heat absorption during the dehydration transformation of $\text{Ce}(\text{OH})_3$ to CeO_2 .

The N_2 -sorption isotherm curves of as-prepared LDOs materials all exhibited typical type-IV behavior, and there was

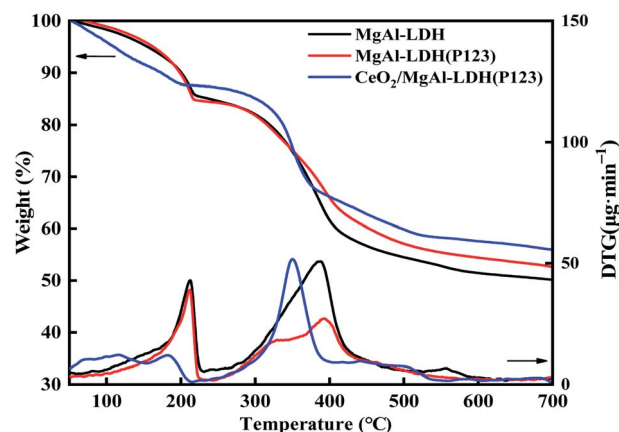
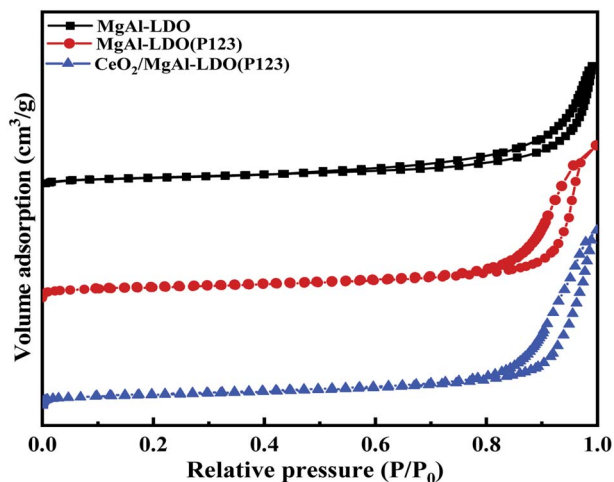
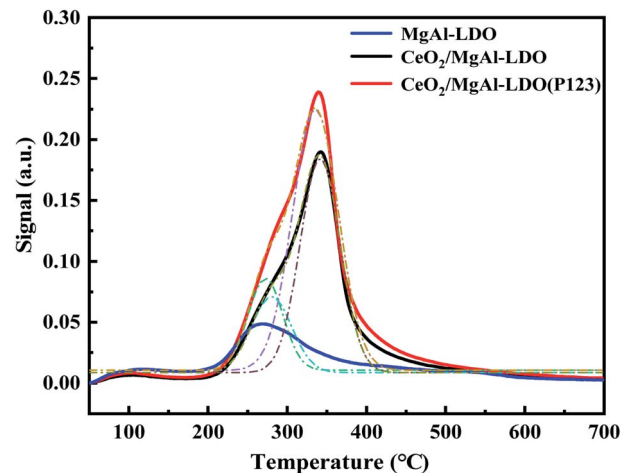


Fig. 5 TG-DTG curves of as-prepared materials.



Fig. 6 N₂ adsorption-desorption isotherms of as-prepared materials.Fig. 7 CO₂-TPD spectra of as-prepared materials.

an obvious H3-type hysteresis loop in the range of $P/P_0 > 0.8$, indicating the existence of mesoporous structures in LDOs materials (Fig. 6).³³ Compared with MgAl-LDO, MgAl-LDO(P123) had significantly increased specific surface area (SSA), total pore volume and average pore size (Table 1), which is in accordance with the expected modification of the template agent P123. However, the CeO₂/MgAl-LDO(P123) obtained by Ce doping modification of MgAl-LDO(P123) exhibited a slight decrease in SSA, total pore volume and average pore diameter, which may be due to the fact that the Ce introduction would partially cover the surface of the MgAl composite oxide and even enter into its mesoporous channels and skeleton. Comparing the N₂-sorption results of different P123 additions (Fig. S4† and Table 1), it can be found that with the increase of P123 content, the SSA and pore volume of CeO₂/MgAl-LDO(P123) series samples first increased and then decreased, which is due to the fact that higher P123 concentration could inhibit the formation of mesopores.¹⁷ The CeO₂/MgAl-LDO(P123) sample prepared with 1.5% P123 has the largest SSA and pore volume.

Table 1 Textural properties of the DMC catalysts

Sample	S_{BET}^a (m ² g ⁻¹)	Pore volume ^b (cm ³ g ⁻¹)	D_{BJH}^b (nm)
MgAl-LDO	99.61	0.85	16.96
MgAl-LDO(P123)	238.73	1.44	24.12
CeO ₂ /MgAl-LDO (P123)	199.57	1.37	23.23
CeO ₂ /MgAl-LDO (1.0%P123)	155.68	1.09	21.58
CeO ₂ /MgAl-LDO (2.0%P123)	117.88	0.95	23.80
CeO ₂ /MgAl-LDO (2.5%P123)	104.26	0.88	23.50

^a *t*-plot method. ^b Barrett-Joyner-Halenda (BJH) method (the adsorption branch).

The strength and amount of basic sites of LDOs were analyzed *via* CO₂-TPD. Three main CO₂-desorption peaks appeared in the spectrum (Fig. 7), corresponding to weak basic sites (50–200 °C), medium basic sites (200–400 °C) and strong basic sites (500–600 °C), respectively. The weak basic sites were assigned to OH⁻ groups, moderate ones were associated with Mg–O and Al–O, and strong ones were related to coordinatively unsaturated O²⁻ ions, respectively.³⁴ The weak basic sites of CeO₂/MgAl-LDO and CeO₂/MgAl-LDO(P123) were similar to those of MgAl-LDO(P123), but an obvious overlapping peak appeared at the medium basic sites. After peak fitting, the absorption peak around 300 °C may be caused by the adsorption of CO₂ by aluminum hydroxide and MgO,³⁵ while the absorption peak around 350 °C is caused by the oxygen vacancies formed by the introduction of Ce. In addition, from Table 2, we can see that the total base amount of CeO₂/MgAl-LDO(P123) and CeO₂/MgAl-LDO increased significantly after Ce doping, and CeO₂/MgAl-LDO(P123) has the largest amount ones. Combined with the SEM results, it may be due to the fact that the addition of Ce *via* aqueous reconstruction method improved the catalyst morphology, resulting in significantly more edges and defects, thus exposing more basic sites. According to the literature,³⁶ the medium basic site was a key

Table 2 The amount of basic sites of different samples

Samples	Maximum temperature (°C)	Quantity (cm ³ g ⁻¹ STP)
MgAl-LDO	106.32	5.24
	270.52	40.81
	539.09	0.36
CeO ₂ /MgAl-LDO	104.76	3.76
	349.72	187.94
	550.38	6.44
CeO ₂ /MgAl-LDO(P123)	104.06	3.80
	346.47	222.72
	551.09	11.99



factor in the synthesis of propylene glycol methyl ether (PGME), so it is presumed that the same effect should be present in its polymer synthesis.

The state and distribution of surface elements of the $\text{CeO}_2/\text{MgAl-LDO(P123)}$ catalyst were further determined using XPS. Fig. 8 shows the full spectrum of $\text{CeO}_2/\text{MgAl-LDO(P123)}$ and the Ce 3d XPS spectrum. In Fig. 8b, the two characteristic peaks at 900 eV and 882 eV were assigned to the Ce 3d³ and Ce 3d⁵ orbital electron energy levels, respectively. Among them, Ce 3d_{3/2} multiple signals were labeled with μ_0 , μ_1 , μ_2 , and Ce 3d_{5/2} were labeled with ν_0 , ν_1 , ν_2 . These six peaks were attributed to the typical characteristic peaks of Ce(IV).^{30,37,38} The characteristic peaks of Ce(III) at 903 eV and 885 eV had lower response values, indicating that Ce(III) and Ce(IV) co-exist in the surface composition of the material, but Ce(IV) is the main form, *i.e.*, CeO_2 instead of Ce_2O_3 . For CeO_2 catalysts, Ce(IV) is the dominant valence state and a key factor in catalyst activity.

3.2 Catalytic synthesis of MPPG

MPPG is widely used in coatings, inks, printing and dyeing, cleaning agents and other industries, and has been widely used in the formulation of automotive brake fluids and brake fluids for hydraulic transmission machinery in recent years. The synthesis mechanism of polyether polyols from PO catalyzed by heterogeneous solid base catalysts has been reported.^{39,40} Combined with the basic properties of LDOs, the reaction process of MPPG can be described as shown in Scheme 1. The basic sites in LDOs formed dormant sites with the initiator methanol (Induction period). Next, the monomer PO interacts with the coordination unsaturated Mg^{2+} in the LDOs to activate the ring opening. Due to the steric hindrance effect of PO, the primary carbon of PO is mainly attacked (Chain initiation). Then, the growing polymer continues to nucleophilically attack PO, thereby realizing the growth of the polymer chain (chain growth). Finally, the reaction was terminated until the PO was exhausted (chain termination).

In this work, the catalytic activity of the as-prepared different materials was evaluated *via* the synthesis of MPPG from methanol and PO. Under the same reaction conditions that the molar ratio is 1 : 7 between methanol and PO, the catalyst dosage is 5%, the pressure is 1.5 MPa, the temperature is 140 °C, the stirring rate is 350 rpm and the reaction time is 6 h, the catalytic

results of different as-prepared materials are shown in Table 3. Obviously, the catalytic performances of LDOs materials were all better than that of their precursor LDHs, and the $\text{CeO}_2/\text{MgAl-LDO(P123)}$ obtained by introducing P123 and Ce showed the best catalytic performance. Based on the characterization results above, the CO_2 -TPD results show that the introduction of Ce improves the acid-base properties of LDOs, leading to a significant increase in medium to strong basic sites, and $\text{CeO}_2/\text{MgAl-LDO(P123)}$ has the most medium basic sites. On the other hand, the N_2 -sorption analysis demonstrated that the introduction of P123 significantly improved the SSA and pore volume of LDOs. In addition, the introduction of Ce by the aqueous reconstruction method allows LDOs to exhibit more structural defects, thus facilitating the exposure of more active sites.

Moreover, the previous study of our research group⁴¹ found that the aggregation of CeO_2 particles would affect the catalytic performance of the catalyst, and the doping amount of Ce in the LDOs material should not be too large, so we optimized the doping amount of Ce through experiments as well (Fig. 9a). It can be seen that the catalyst activity was the best when the content of CeO_2 in the catalyst was 16 wt%. Meanwhile, Fig. 9b also shows that the optimal addition amount of P123 is 1.5 wt%. The results of N_2 -sorption characterization showed that the $\text{CeO}_2/\text{MgAl-LDO(P123)}$ sample prepared with 1.5% P123 addition had the highest SSA and pore volume. Finally, the process conditions for the polymerization to generate MPPG were also discussed, as shown in Fig. 10. The results showed that too long reaction time, high reaction temperature and reaction pressure could affect the quality of the products. This is because exceeding certain ratios or conditions could cause side reactions that can increase the molecular weight distribution and colour of the product. After single-factor optimization (Fig. 10), a molar ratio between methanol and PO was 1 : 7, PO conversion of 92.04% was achieved at 1.5 MPa, 350 rpm and 140 °C for 7 h using 5.0 wt% $\text{CeO}_2/\text{MgAl-LDO(P123)}$ catalyst. At this point, the Mn of MPPG reached 405 and the polymer dispersion index was 1.04.

Finally, FTIR (Fig. 11) and ^1H NMR (Fig. 12) were used to analyze the functional groups and structures of the product MPPG and compared with standard samples. In Fig. 11, the absorption peak of the terminal hydroxyl group (–OH) appeared

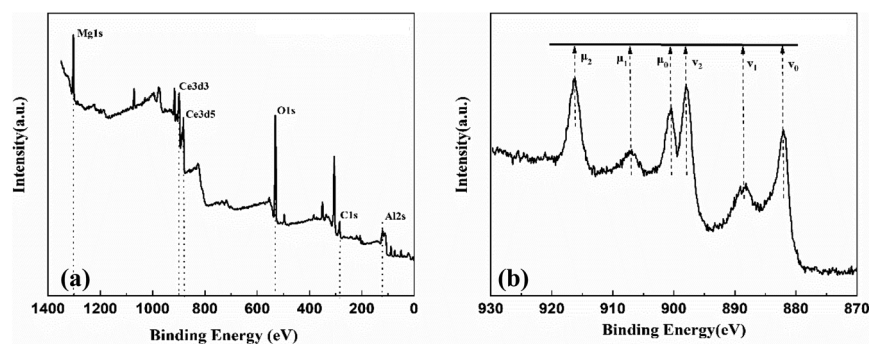
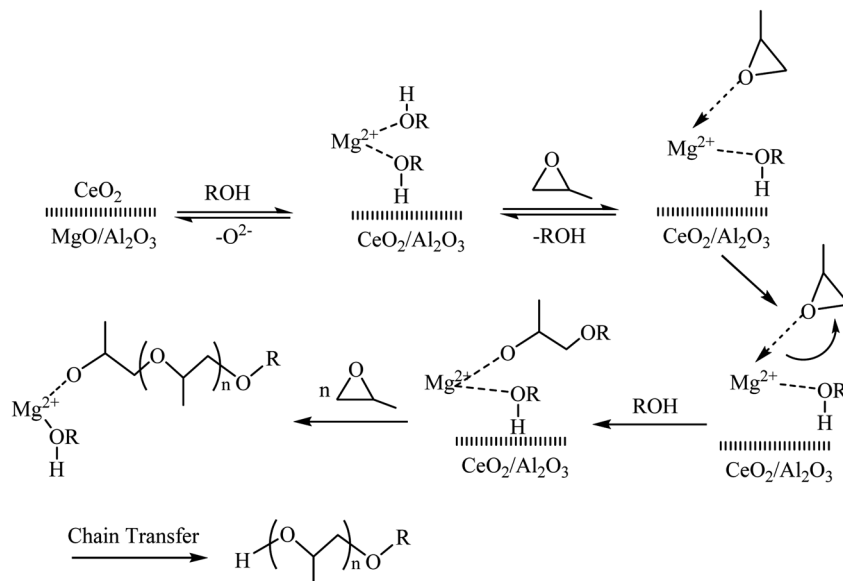


Fig. 8 (a) The XPS survey spectrum of $\text{CeO}_2/\text{MgAl-LDO(P123)}$; (b) the Ce 3d spectrum.





Scheme 1 Mechanism of PO polymerization catalyzed by LDOs.

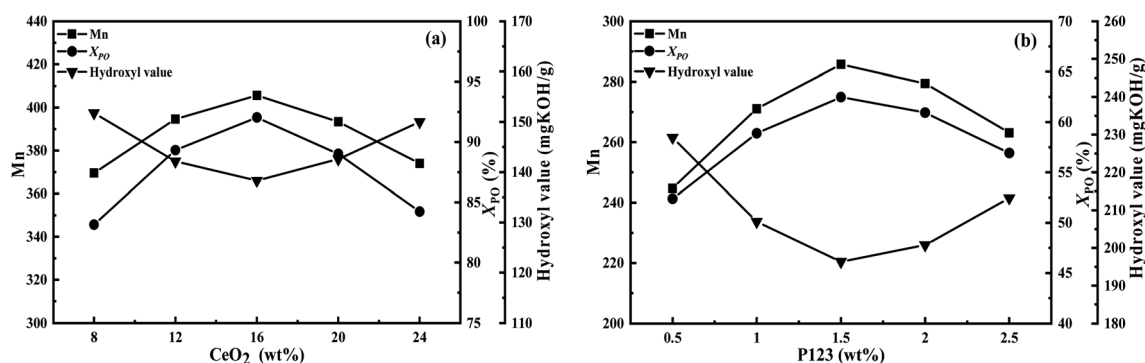
around 3480 cm^{-1} . The antisymmetric and symmetric stretching vibration peaks of methyl group ($-\text{CH}_3$) appeared at 2971 cm^{-1} and 2866 cm^{-1} , while the deformation vibration

peaks of $-\text{CH}_3$ appeared at 1456 cm^{-1} and 1374 cm^{-1} . The absorption peaks of ether bonds ($\text{C}-\text{O}-\text{C}$) appeared at 1100 cm^{-1} and 931 cm^{-1} , which were characteristic peaks for

Table 3 Catalytic activity for the synthesis of MPPG on different catalysts^a

Catalyst	PO/Me (mol mol ⁻¹)	X_{PO} (%)	Mn^b	PDI^c	OHV^d (mgKOH g ⁻¹)
Al_2O_3	7	24.13	130	1.12	432.07
MgO	7	36.47	180	1.12	311.56
MgAl-LDH	7	42.08	203	1.10	276.57
MgAl-LDH (P123)	7	40.11	195	1.08	287.92
$\text{CeO}_2/\text{MgAl-LDH}$	7	54.21	252	1.08	222.53
$\text{CeO}_2/\text{MgAl-LDH}$ (P123)	7	62.88	287	1.06	195.27
MgAl-LDO	7	53.16	248	1.06	226.37
MgAl-LDO (P123)	7	62.49	286	1.05	196.35
$\text{CeO}_2/\text{MgAl-LDO}$	7	81.08	361	1.05	155.32
$\text{CeO}_2/\text{MgAl-LDO}$ (P123)	7	92.04	405	1.04	138.28
42KOH*	6.2	—	280	—	199.80

^a The maximum standard deviation of each data was <2.0%. ^b Number average molecular weight measured by GPC in THF. ^c PDI = polymer dispersity index, determined by GPC in THF. ^d Determined by national standard method.

Fig. 9 Effect of CeO_2 (a) and P123 (b) content on catalytic performance.

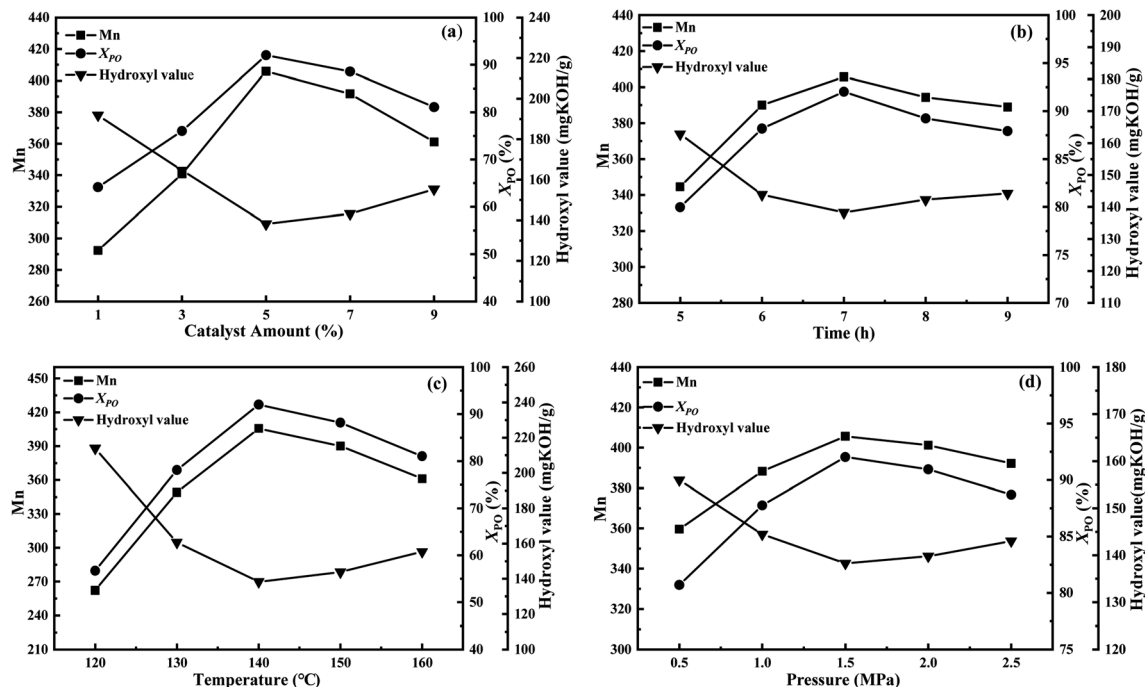


Fig. 10 Single-factor optimization of the polymerization reaction: (a) catalyst amount, (b) reaction time, (c) reaction temperature, and (d) reaction pressure.

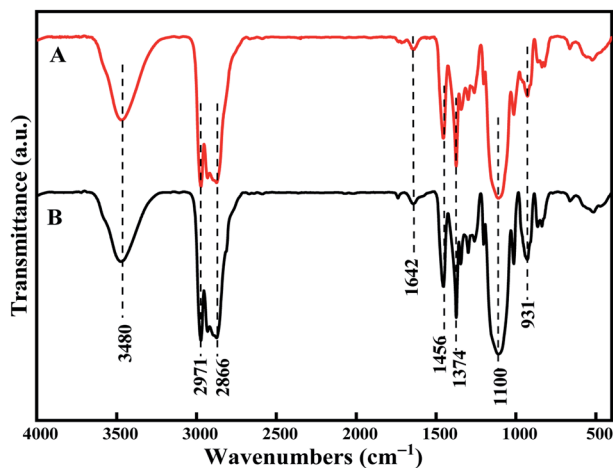


Fig. 11 FTIR spectrum of PPG product. (A): the synthetic product of MPPG, (B): the standard sample of MPPG.

identifying polyether compounds. In addition, an unsaturated double bond ($\text{C}=\text{C}$) absorption peak appeared at 1642 cm^{-1} with a relatively weak peak intensity, indicating that the prepared MPPG sample was less unsaturated. The peak positions and shapes of the MPPG products synthesized in this work are basically the same as those of the MPPG standard sample in the NMR spectra, and the peak positions are mainly divided into two parts: $\delta 1.05\text{--}\delta 1.08\text{ ppm}$ and $\delta 2.8\text{--}\delta 3.9\text{ ppm}$ (Fig. 12). The peaks in the region of $\delta 1.05\text{--}\delta 1.08\text{ ppm}$ (a) were assigned to the absorption peaks of methyl ($-\text{CH}_3$) protons on the polymer repeating unit segments. The peaks in the $\delta 2.8$ to $\delta 3.9$ region

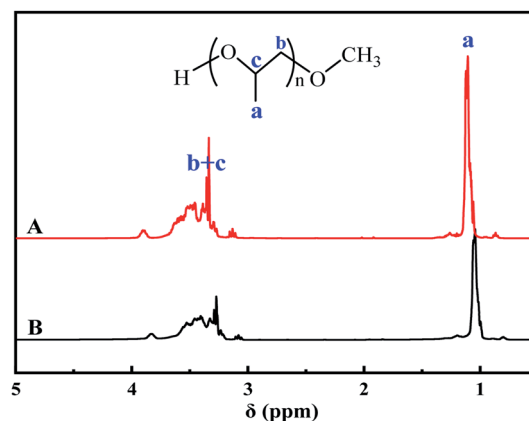


Fig. 12 ^1H NMR spectrum of MPPG product. (A): the synthetic product of MPPG, (B): the standard sample of MPPG.

belong to the hydrogen nucleus absorption peaks on methylene ($-\text{CH}_2$) and methine ($-\text{CH}$) protons (b, c).

3.3 Catalyst life test

For heterogeneous catalysts, its lifetime is an important indicator, and multiple recycling can save production costs. The reusability of the $\text{CeO}_2/\text{MgAl-LDO}(\text{P123})$ solid base catalyst was investigated under optimal reaction conditions for the polymerization to produce MPPG. After the reaction, the catalyst was filtered out, washed repeatedly with distilled water and ethanol to remove the residual MPPG on the catalyst, then dried and calcined, and continued to be used for the synthesis of



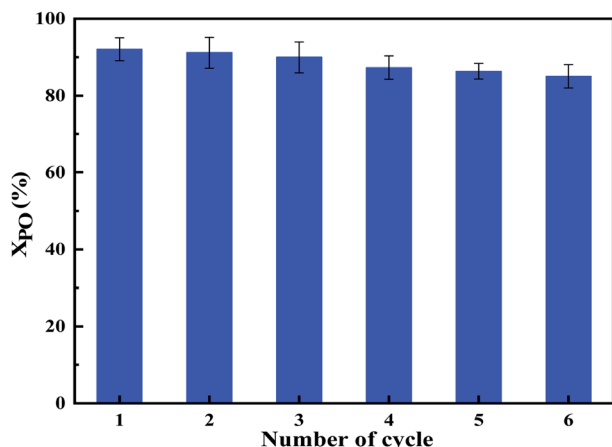


Fig. 13 Recycling test (reaction between PO and methanol in the presence of CeO₂/MgAl-LDO (P123)).

MPPG. As shown in Fig. 13, the conversion of PO can still reached 83.69% after being used six times. This phenomenon indicated that the CeO₂/MgAl-LDO(P123) catalyst had good recycling performance due to the “memory function” of the hydrotalcite-like materials on one hand, thereby allowed its morphological structure to be recovered under certain circumstances to retain more active sites. On the other hand, based on the N₂-sorption and CO₂-TPD analysis, CeO₂/MgAl-LDO(P123) had more basic sites and specific surface area, which can supply enough active sites for MPPG polymerization process. The significantly improved mesopore volume can facilitate the diffusion of macromolecules, thereby alleviating the deactivation of the catalyst.

4 Conclusions

In this work, CeO₂/MgAl-LDH(P123) was prepared by a two-step method using nucleation/crystallization isolation method and aqueous reconstruction method, and the CeO₂/MgAl-LDO(P123) catalyst obtained by calcining its precursor was applied in synthesis of MPPG. Under the optimal reaction conditions, the conversion rate of PO reached 92.03%, and the Mn of MPPG reached 405. The introduction of the template agent P123 significantly raised the specific surface area and pore volume of the LDOs material. On the other hand, the presence of CeO₂ leads to the formation of oxygen vacancies, enriching the moderately basic sites. Furthermore, the modification of P123 and Ce changed the size of LDOs and the structure became fine and loose, which facilitated the exposure of more active sites. Thus, CeO₂/MgAl-LDO(P123) exhibited high activity in the polymerization to generate MPPG compared to unmodified LDOs. This research provides guidance for the industrial application of MPPG production using heterogeneous catalysts.

Funding information

The authors acknowledge financial support from the National Natural Science Foundation of China (21973045), China

Petroleum & Chemical Corporation (J418013-3) and Jiangsu scientific and technological transformative project (SBA2018030374). The related measure and analysis instrument for this work were supported by Centre for Analysis, Nanjing Normal University.

Conflicts of interest

The authors declare that they have no conflicts of interest.

References

- H. Gu, R. B. Sheng, Y. L. Huang and X. G. Chen, Chinese high-tech enterprise, 2009, 2, in Chinese.
- W. Bing and M. Wei, *J. Solid State Chem.*, 2019, **269**, 184–194.
- Q. Wang and D. O'Hare, *Chem. Rev.*, 2012, **112**, 4124–4155.
- G. Fan, F. Li, D. G. Evans and X. Duan, *Chem. Soc. Rev.*, 2014, **43**, 7040–7066.
- J. Yu, Q. Wang, D. O'Hare and L. Sun, *Chem. Soc. Rev.*, 2017, **46**, 5950–5974.
- X. Duan and D. G. Evans, *Struct. Bonding*, 2006, 193–223.
- M. V. Bukhtiyarova, *J. Solid State Chem.*, 2019, **269**, 494–506.
- F. Cavani, F. Trifirò and A. Vaccari, *Catal. Today*, 1991, **11**, 173–301.
- B. F. Sels, D. E. De Vos and P. A. Jacobs, *Catal. Rev.*, 2001, **43**, 443–488.
- J. Feng, Y. He, Y. Liu, Y. Du and D. Li, *ChemInform*, 2015, **46**, 5291–5319.
- L. Mohapatra and K. Parida, *J. Mater. Chem. A*, 2016, **4**, 10744–10766.
- C. Del Hoyo Martínez, *Appl. Clay Sci.*, 2007, **36**, 103–121.
- P. Kuśtrowski, D. Sułkowska, L. Chmielarczyk, A. Rafalska-Łasocha, B. Dudek and R. Dziembaj, *Microporous Mesoporous Mater.*, 2005, **78**, 11–22.
- P. Pinthong, P. Praserttham and B. Jongsomjit, *J. Oleo Sci.*, 2019, **68**, 95–102.
- L.-B. Sun, X.-Q. Liu and H.-C. Zhou, *Chem. Soc. Rev.*, 2015, **44**, 5092–5147.
- P. Tan, Z. Gao, C. Shen, Y. Du, X. Li and W. Huang, *Chin. J. Catal.*, 2014, **35**, 1955–1971.
- J. Wang, J. Zhou, Z. Li, Y. He, S. Lin, Q. Liu, M. Zhang and Z. Jiang, *J. Solid State Chem.*, 2010, **183**, 2511–2515.
- D. Martin and D. Duprez, *J. Mol. Catal. A: Chem.*, 1997, **118**, 113–128.
- A. Trovarelli, *Catal. Rev.*, 1996, **38**, 439–520.
- B. Jiang, Z. Xi, F. Lu, Z. Huang, Y. Yang, J. Sun, Z. Liao, J. Wang and Y. Yang, *Catal. Sci. Technol.*, 2019, **9**, 6335–6344.
- S. Nayak and K. M. Parida, *Int. J. Hydrogen Energy*, 2016, **41**, 21166–21180.
- D. Cabrera-Munguia, H. González, M. Barreto-Gutiérrez, A. Gutierrez-Alejandre, J. L. Rico and D. Solis, *Catal. Lett.*, 2020, **150**, 1957–1969.
- H. M. S. Al-Aani, E. Iro, P. Chirra, I. Fechete, M. Badea, C. Negrilă, I. Popescu, M. Olea and I.-C. Marcu, *Appl. Catal., A*, 2019, **586**, 117215.
- A. Faour, V. Prévot and C. Taviot-Gueho, *J. Phys. Chem. Solids*, 2010, **71**, 487–490.



- 25 M. E. Manríquez, I. Elizalde and E. Ortiz, *React. Kinet., Mech. Catal.*, 2020, **131**, 1–12.
- 26 D. Cosano, J. Hidalgo-Carrillo, D. Esquivel, F. Romero, C. Jiménez-Sanchidrián and J. R. Ruiz, *J. Porous Mater.*, 2020, **27**, 441–450.
- 27 L. Wang, J. Ding, Y. Chai, Q. Liu, J. Ren, X. Liu and W. Dai, *Dalton Trans.*, 2015, **44**, 11223–11234.
- 28 J. Hong, Y. Wang, J. Pan, Z. Zhong and R. Xu, *Nanoscale*, 2011, **3**, 4655–4661.
- 29 N. N. A. H. Meis, J. H. Bitter and K. P. de Jong, *Ind. Eng. Chem. Res.*, 2010, **49**, 1229–1235.
- 30 W. L. J. Kwok, D.-G. Crivoi, C. Chen, J.-C. Buffet and D. O'Hare, *Dalton Trans.*, 2018, **47**, 143–149.
- 31 O. Dan, E. Butenko and A. Kapustin, *Chem.-Didact.-Ecol.-Metrol.*, 2018, **23**, 137–142.
- 32 H. Nguyen, H. Nguyen, D. Dao and L. Hoang, *J. Porous Mater.*, 2017, **23**, 1–10.
- 33 C. Marquez, M. Rivera-Torrente, P. P. Paalanen, B. M. Weckhuysen, F. G. Cirujano, D. De Vos and T. De Baerdemaeker, *J. Catal.*, 2017, **354**, 92–99.
- 34 G. Wu, X. Wang, B. Chen, J. Li, N. Zhao and Y. Sun, *Appl. Catal., A*, 2007, **329**, 106–111.
- 35 F. Liu, Y. Xiao, X. Sun, G. Qin, S. Xiuyang and Y. Liu, *Chem. Eng. J.*, 2019, **369**, 205–214.
- 36 W. Zhang, H. Wang, W. Wei and Y. Sun, *J. Mol. Catal. A: Chem.*, 2005, **231**, 83–88.
- 37 G. M. Ingo, R. D. Maschio and L. Scoppio, *Surf. Interface Anal.*, 2010, **18**, 661–666.
- 38 S. Hu, F. Zhou, L. Wang and J. Zhang, *Catal. Commun.*, 2011, **12**, 794–797.
- 39 T. Biedron, P. Kubisa and S. Penczek, *J. Polym. Sci., Part A: Polym. Chem.*, 1991, **29**, 619–628.
- 40 C. Tran, L. Pham, Y. Lee, H. Jang, S. A. Kim and I. Kim, *J. Catal.*, 2019, **372**, 86–102.
- 41 K. Wang, Q. Mao, W. Fei, L. Kong, X. Cao and Z. Gu, *RSC Adv.*, 2021, **11**, 8375–8383.
- 42 X. Jing, R. Rong, W. Dong and Y. Sun, [P], CN105237758A.

